Mechanism of Nucleotide Release from Rho by the GDP Dissociation Stimulator Protein

Jon P. Hutchinson and John F. Eccleston*

Division of Physical Biochemistry, National Institute for Medical Research, The Ridgeway, Mill Hill, London NW7 1AA, U.K.

Received April 3, 2000; Revised Manuscript Received June 21, 2000

ABSTRACT: Guanine nucleotide dissociation stimulator (GDS) promotes the release of tightly bound GDP from various Ras superfamily proteins, including RhoA, Rac1, K-Ras, Rap1A, and Rap1B. It displays no significant sequence homology to other known exchange factors for small G-proteins. Studies are reported here of the mechanism of GDS-mediated nucleotide release from RhoA using a combination of equilibrium and stopped-flow kinetic measurements, employing fluorescent *N*-methylanthraniloyl (mant) derivatives of GDP and 2′-deoxyGDP. It is proposed that GDS operates by an associative displacement mechanism where stimulated nucleotide release from the Rho·mantGDP complex occurs via a transiently populated ternary complex (Rho·GDS·mantGDP). In kinetic experiments where excess GDS was mixed with the Rho·mantGDP complex, stimulated mantGDP dissociation rates of 1 s^{-1} were measured during a single turnover, representing a 5000-fold enhancement over the intrinsic rate of mantGDP dissociation from Rho. The stable, nucleotide-free binary complex Rho·GDS was isolated. When the Rho·GDS complex was mixed with excess mantGDP, a biphasic increase in fluorescence occurred, the observed rate constants of which both reached saturating values at high mantGDP concentrations. This is compelling evidence that an isomerization of the Rho·GDS·mantGDP ternary complex is an important feature of the mechanism of nucleotide release.

Members of the Ras superfamily of small GTP-binding proteins (G-proteins) are fundamental components of cellular signal transduction pathways and have been shown to regulate a wide variety of biological processes (*1*). These highly conserved proteins can be assigned to different subfamilies on the basis of primary structural homology. The action of small G-proteins is characterized by their ability to switch between a biologically inactive GDP-bound conformation and an active GTP-bound conformation which can interact with downstream effectors. Cycling between these two states is governed by the rates of GTP hydrolysis and GDP dissociation, both of which are intrinsically very slow. Various accessory proteins have been identified which act as regulators of this cycle (*2*). GTPase activating proteins (GAPs) accelerate GTP hydrolysis and thus lower the population of the active conformation. Guanine nucleotide exchange factors (GEFs) promote exchange of tightly bound GDP for GTP, thus increasing the active population. Many of the exchange factors identified for small G-proteins are large proteins comprising various functional domains. Domains possessing exchange activity typically exhibit extensive structural diversity and are usually specific to individual small G-protein subfamilies. For example, Cdc25 and Sos, which share a homologous catalytic domain, have been identified as exchange factors for Ras subfamily proteins, and DH domain proteins have exchange activity against members of the Rho subfamily (*3*).

Guanine nucleotide dissociation stimulator (GDS)[1] was originally isolated from the cytosol of bovine brain as a positive regulator of Rap1, a Ras subfamily protein (*4*). Its precise physiological role is currently unknown. GDS is composed of 558 residues (molecular mass of 61 kDa) and shows no significant sequence homology to other known GEFs. Virtually the entire sequence is composed of 11 repeats of a 42-amino acid motif first identified in the *Drosophila* armadillo protein, a homologue of β-catenin (*5*). The repeats in β-catenin, which each comprise three helices, are sequentially packed into an elongated structure (*6*). Interestingly, the catalytically active Sec7 domain of ARNO, an exchange factor for human Arf1, comprises 10 α-helices which are arranged into an approximately cylindrical tertiary structure (*7*, *8*). This superfold bears some similarity to that of the armadillo repeat region.

In contrast to other known nucleotide exchange factors for small G-proteins, GDS displays a broad substrate specificity. Activity has been detected in vitro against members from different small G-protein subfamilies, including Rap1A, Rap1B, and K-Ras of the Ras subfamily and RhoA, Rac1, and Cdc42 of the Rho/Rac subfamily (*9*, *10*). Known substrates possess a C-terminal polybasic region which has been suggested to be involved in recognition by GDS (*11*). Early studies indicated that GDS was only active against small G-proteins which were post-translationally modified (*11*). However, this has been shown not to be an absolute requirement since GDS activity has been detected against the unmodified forms of RhoA and to a lesser extent

* To whom correspondence should be addressed. Telephone: 44-208 959 3666. Fax: 44-208 906 4419. E-mail: jeccles@nimr.mrc.ac.uk.

[1] Abbreviations: GDS, guanine nucleotide dissociation stimulator; mantGDP, 2′(3′)-*O*-*N*-methylanthraniloyl GDP; mant*d*GDP, 2′-deoxy-3′-*O*-*N*-methylanthraniloyl GDP; ANS, 8-anilino-1-naphthalenesulfonic acid; DTT, dithiothreitol.

10.1021/bi0007573 CCC: $19.00
Published on Web 08/23/2000

Cdc42 and Rac1 (*10*). As well as promoting GDP dissociation, GDS has also been proposed to regulate the translocation of lipid-modified small G-proteins by inhibiting their association with membranes (*12*).

It is unclear whether exchange factors with diverse structure operate by a common mechanism. The first characterized nucleotide exchange factor, EF-Ts, catalyzes GDP dissociation from the prokaryotic protein biosynthetic elongation factor Tu (EF-Tu). Detailed kinetic studies have established that nucleotide dissociation is catalyzed in a substituted enzyme mechanism (*13*−*17*). EF-Ts associates with the EF-Tu·GDP complex to form a ternary complex from which GDP dissociates at a rate higher than its rate of dissociation from EF-Tu. Nucleotide exchange is then completed by the association of GTP with the EF-Tu·EF-Ts binary complex followed by EF-Ts dissociation. The exchange process is likely to be driven by the ∼30-fold higher cellular concentration of GTP compared to the concentration of GDP (*18*). The structure of the binary complex between Ras and its exchange factor Sos shows that Sos functions by inducing a large conformational change in Ras which opens up the nucleotide binding site. This, together with the direct interaction of certain residues from Sos, interferes with the binding of the nucleotide-associated magnesium ion and phosphate groups, thus lowering the affinity for nucleotide (*19*).

More recently, an analogous mechanism has been established for RCC1, an exchange factor for Ran (*20*, *21*), and the catalytic domain of $Cdc25^{Mm}$, an exchange factor for Ras (*22*). However, a more complex mechanism has been suggested for the catalysis of GDP release from the eukaryotic initiation factor 2 (eIF-2) by the exchange factor, eIF-2B. In the proposed sequential mechanism, a quaternary complex eIF-2·GDP·eIF-2B·GTP is formed, which invokes a nucleotide binding site on the exchange factor (*23*).

In this paper, we describe detailed equilibrium and kinetic measurements aimed at defining the mechanism by which GDS stimulates the dissociation of GDP from RhoA. Environmentally sensitive fluorescent *N*-methylanthraniloyl (mant) derivatives of GDP as well as intrinsic tryptophan fluorescence and extrinsic ANS fluorescence were used as probes. Mant derivatives of nucleotides, typically labeled at the ribose hydroxyls, have been extensively used in mechanistic studies of GTPases and ATPases (*24*).

Data obtained for the interaction of GDS with Rho·mantGDP and for the interaction of mantGDP with Rho·GDS are consistent with a mechanism where a Rho·GDS·mantGDP ternary complex is transiently populated. Kinetic data indicate that a conformational change occurs within this ternary complex, and the rate constants of the interconversion of the two conformational states could be resolved. Previous studies on nucleotide exchange factors which operate by ternary complex formation have proposed a conformational change within this complex (*17*, *21*, *22*), which may represent an intrinsic feature of the mechanism of stimulated nucleotide exchange.

MATERIALS AND METHODS

Preparation of Proteins. Human RhoA was expressed as a GST fusion in *Escherichia coli* strain BL21 using the pGEX-2T expression vector (Amersham Pharmacia). The recombinant RhoA contains a point mutation (F25N) to improve stability and was cloned without the N-terminal methionine (*25*). After thrombin cleavage, the protein bears three extra N-terminal residues (Gly-Ser-Pro). Cell growth, induction, and lysis were performed in a manner similar to that described previously for GDS (*26*). After the soluble fraction had been passed over a column of 20 mL of glutathione-Sepharose and washed to baseline absorption, human thrombin (400 units) was cycled over the column at a rate of 0.5 mL/min overnight to cleave the fusion. The protein was eluted, passed over a column of *p*-aminobenzamidine-agarose, and concentrated by ultrafiltration (Amicon YM10 membrane). RhoA·GDP was further purified on an S-75 gel-filtration column (60 cm × 2.6 cm, injection volume of 3 mL) equilibrated in 20 mM Tris-HCl, 50 mM NaCl, 2 mM $MgCl_2$, and 1 mM DTT (pH 7.5) at a flow rate of 1.5 mL/min. After concentration to approximately 10 mg/mL, the protein was snap-frozen in aliquots and stored at −80 °C. Approximately 100 mg of RhoA was obtained from 30 g wet weight of cells. The purity was estimated to be in excess of 95% as judged by Coomassie blue-stained SDS−polyacrylamide gels. Electrospray mass spectrometry gave the anticipated molecular weight of 21 845. Concentrations of Rho·GDP were determined by absorbance using an ϵ_{280} of 26 430 M^{-1} cm^{-1}, which is calculated from the amino acid composition and a stoichiometrically bound equivalent of GDP.

Full-length GDS and the Rho·GDS complex were prepared and characterized as described previously (*26*). Concentrations of GDS and Rho·GDS were determined by absorbance using an ϵ_{280} of 13 940 M^{-1} cm^{-1} and an ϵ_{280} of 31 720 M^{-1} cm^{-1}, respectively, which are calculated from the amino acid composition.

Preparation of Rho·MantGDP, Rho·MantdGDP, and Rho·[^{3}H]GDP. MantGDP and mant*d*GDP were synthesized, purified, and characterized as described previously (*24*, *27*) except that a 2-fold excess of *N*-methylisatoic anhydride was used. Rho·mant-nucleotide complexes were prepared by incubating Rho·GDP with mantGDP or mant*d*GDP (50-fold excess) in 20 mM Tris-HCl, 40 mM EDTA, 200 mM $(NH_4)_2SO_4$, and 1 mM DTT (pH 7.5) at room temperature for 10 min. Exchange was then quenched by addition of $MgCl_2$ to a final concentration of 50 mM, and the complex was separated from free nucleotide by gel filtration on a PD-10 column (Amersham Pharmacia) eluted with 20 mM Tris-HCl, 2 mM $MgCl_2$, and 1 mM DTT (pH 7.5) (standard buffer) at 4 °C. Rho·mant-nucleotide complex concentrations were determined by absorbance using the extinction coefficient of the mant fluorophore [ϵ_{354} = 5700 M^{-1} cm^{-1} (*27*)].

Rho·[^{3}H]GDP was prepared by incubating 0.5 mg of Rho·GDP with [^{3}H]GDP (600 kBq, 437 GBq/mmol, Amersham) in 20 mM Tris-HCl, 40 mM EDTA, 200 mM $(NH_4)_2SO_4$, and 1 mM DTT (pH 7.5) at room temperature for 10 min. Exchange was quenched by addition of $MgCl_2$ to a final concentration of 50 mM, and the complex was separated from free nucleotide on a FastDesalt HR10/10 column (Amersham Pharmacia) equilibrated in standard buffer at a rate of 0.5 mL/min. Elution was monitored by absorption and radioactivity. The concentration of Rho·[^{3}H]GDP was determined spectroscopically as described for Rho·GDP. The specific activity of Rho·[^{3}H]GDP prepared by this method was approximately 470 cpm/pmol when counted in 5 mL Beckman "ReadySafe" scintillation fluid using a Beckman LS6000SC counter.

Fluorescence Measurements. All equilibrium and kinetic measurements were taken at 30 °C in a buffer of 20 mM Tris-HCl, 2 mM $MgCl_2$, and 1 mM DTT (pH 7.5). Equilibrium measurements were carried out using an SLM 8000S photon-counting spectrofluorimeter (SLM Instruments, Urbana, IL), using 4 mm square quartz cuvettes in a thermostatically controlled holder. Intensity data were obtained with the instrument in the L-format, monitoring emission through a monochromator. For long time-base experiments and titrations, data were collected manually and the shutters closed between readings to minimize photobleaching. The observed intensity values were corrected for fluctuations in photomultiplier response and lamp intensity by normalizing measurements to those of a reference sample contained in a second cuvette. Anisotropy measurements were taken in the T-format, where parallel and perpendicular components of the emitted light were monitored simultaneously through KV399 cutoff filters (Schott). A correction factor for differing photomultiplier responses was obtained by exciting the sample with horizontally polarized light. Anisotropy (*A*) was calculated using eq 1

$$A = (I_{||} - I_{\perp})/(I_{||} + 2I_{\perp}) \quad (1)$$

where $I_{||}$ and $I_{\perp}$ are the emission intensities parallel and perpendicular to the vertically polarized excitation light, respectively. The total intensity (*I*) was calculated using eq 2.

$$I = I_{||} + 2I_{\perp} \quad (2)$$

Kinetic experiments were carried out with a Hi-Tech SF61MX stopped-flow instrument. Emission was collected through either a Kodak Wratten 2E cutoff filter (mant and ANS fluorescence) or a WG320 cutoff filter (tryptophan fluorescence). Excitation wavelengths were 366 nm for mant and ANS fluorescence and 280 nm for tryptophan fluorescence. Stopped-flow anisotropy measurements were taken on the same instrument in the T-format, enabling the parallel and perpendicular components of emission to be monitored simultaneously. A rotatable polarizer on the excitation path allowed the response of the two photomultipliers to be normalized by exciting the sample with horizontally polarized light before data acquisition. The anisotropy and total intensity were calculated using eqs 1 and 2. An instrumental time constant was selected which was less than 1% of the half-time of the fastest process being measured. Time courses were analyzed by fitting the data to single- or double-exponential functions, incorporating a slope if photobleaching was significant, using the nonlinear fitting routine contained in the Hi-Tech software or the program Grafit version 3.00 (Erithacus Software, Staines, U.K.). The observed rate constants are typically the mean and standard deviation of four to six individually analyzed time courses. Reported concentrations are those in the reaction chamber after mixing. Secondary plots of observed rate constants which displayed a hyperbolic dependency on the concentration of excess reactant under pseudo-first-order conditions were fitted to a simple hyperbolic function (eq 3)

$$k_{obs} = \frac{k_f[X]}{K_{d,app} + [X]} + k_r \quad (3)$$

where [X] is the concentration of excess reactant and $K_{d,app}$ the concentration of X at half-saturation (*28*). The ordinate intercept, k_r, was either fixed at zero or treated as a variable parameter.

Ultrafiltration Assays. Measurement of the concentration of free [^{3}H]GDP in mixtures of Rho·[^{3}H]GDP and GDS was made by partitioning ~10% of the mixture over a Centricon 10 kDa cutoff centrifugal concentrator. Before being used, the concentrator was prepared by centrifuging 1 mL of GDP (5 μM) in standard buffer at 2800*g*. After this initial treatment, and before each separation, the concentrator was rinsed with water, centrifuged with standard buffer (2800*g* for 1 min), and spun in an inverted position to remove buffer from the upper compartment. The filtrate cup was carefully dried with tissue. Assay mixtures (1 mL) were transferred to the concentrator and centrifuged for 1 min at 2800*g*, which resulted in filtration of approximately 100 μL. The amount of radioactivity present in the filtrate was determined by liquid scintillation counting. Background-corrected counts per minute values were converted to [^{3}H]GDP concentration using the measured specific activity of the Rho·[^{3}H]GDP stock with a spectroscopically determined concentration. Control experiments established that the membrane is impermeable to protein-bound [^{3}H]GDP and that GDS in the concentration range that was used had no effect on the partitioning of [^{3}H]GDP. The efficiency of partitioning of [^{3}H]GDP was measured over a range of concentrations. Filtrate [^{3}H]GDP concentrations were observed to be ~85% of the respective retentate concentrations in a range from 5 nM to 50 μM [^{3}H]GDP. Since this depletion was independent of [^{3}H]GDP concentration, filtrate [^{3}H]GDP concentrations measured in the presence of GDS were corrected by this factor to yield an estimate of $[[^3H]GDP]_{free}$ in the retentate. The application of similar methods in studying small molecule−macromolecule interactions has been discussed previously (*29*).

Data Analysis and Simulation. Nonlinear least-squares fitting was performed with the program Grafit version 3.00 (Erithacus Software). Global analysis of equilibrium and kinetic data by numerical methods was performed with the program Scientist version 2.0 (MicroMath Scientific Software, Salt Lake City, UT). These routines are available on request. Kinetic models were simulated using the program KSim (N. C. Millar).

RESULTS

Characterization of the Rho·MantGDP Complex. The binding of mantGDP to Rho causes an ~3.5-fold enhancement in mant emission intensity at 430 nm (20 °C) and a blue shift of ~15 nm in the emission maximum (data not shown). Similar observations have been made for the binding of mantGDP to other small G-proteins such as Ras (*30*). Fluorescence resonance energy transfer was observed between tryptophan in Rho and the mant fluorophore. This has been observed with the small G-protein Ran (*21*) and other protein−mant nucleotide complexes (*31*, *32*). The fluorescence anisotropy of Rho·mantGDP when excited at 366 nm is ~0.180, compared to a value of ~0.025 for the free nucleotide, which is consistent with reduced global and/or local motion of the fluorophore in the complex (*33*).

The intrinsic rate of mantGDP dissociation from Rho was measured in a displacement experiment. The decrease in fluorescence intensity on excitation at 366 nm after mixing

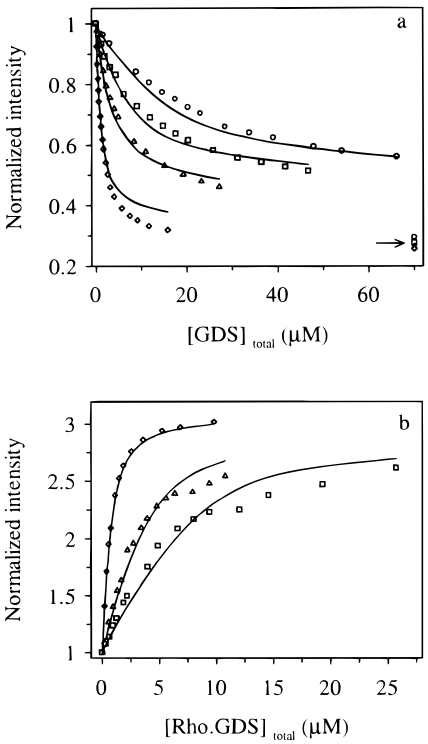

FIGURE 1: Equilibrium titrations of Rho·mantGDP with GDS and mantGDP with Rho·GDS. (a) GDS was titrated into Rho·mantGDP at initial concentrations of 1 (◇), 5 (△), 10 (□), and 20 μM (○). Mant fluorescence intensity (λ_{ex} = 366 nm, λ_{em} = 430 nm) was recorded 5 min after each addition. At the end of each titration, a 100 fold excess of GDP over $[Rho{\cdot}mantGDP]_{initial}$ was added to give the intensity for fully displaced mantGDP. Data for each titration were normalized to an intensity of 1 in the absence of GDS. The data marked with an arrow are the intensity values obtained after addition of the 100-fold excess of GDP and have been normalized as described above and corrected for dilution. (b) Rho·GDS was titrated into mantGDP at initial concentrations of 1 (◇), 5 (△), and 10 μM (□). MantGDP at the appropriate concentration was included in the stock solutions of Rho·GDS to prevent dilution of the nucleotide. Mant fluorescence intensity (λ_{ex} = 366 nm, λ_{em} = 440 nm) was recorded after equilibrium had been reached. Data for each titration were normalized to an intensity of 1 in the absence of Rho·GDS. The solid lines show the best global fit to Scheme 3 as described in the text.

1 μM Rho·mantGDP with 100 μM GDP at 30 °C was well-described by a single exponential, yielding a dissociation rate constant of (2.0 ± 0.2) × 10^{-4} s^{-1} (data not shown). For comparison, the intrinsic rate of dissociation of GDP from Rho was measured by mixing Rho·GDP (2.5 μM) with a large excess of mantGDP (250 μM). Excitation by energy transfer (λ_{ex} = 295 nm) allowed mantGDP binding to Rho to be followed, the rate of which is limited by the slow dissociation of GDP. The observed fluorescence intensity increased exponentially at a rate of (1.2 ± 0.3) × 10^{-4} s^{-1}. The similarity of these dissociation rate constants supports the use of mantGDP as an analogue in these studies.

Interaction of GDS with Rho·MantGDP at Equilibrium. Figure 1a shows data from a series of titrations where increasing concentrations of GDS were added to Rho·mantGDP present at initial concentrations of 1, 5, 10, and 20 μM. After each addition, the system was allowed to reach equilibrium (5 min) and the emission intensity at 430 nm was recorded on excitation of the mant fluorophore at 366 nm. The cumulative added volume was <10% of the total volume, and dilution of the total concentration of Rho·

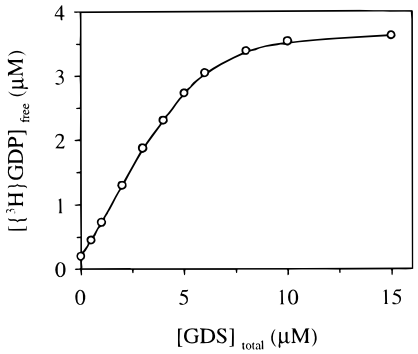

FIGURE 2: Ultrafiltration analysis of [^{3}H]GDP displacement from Rho·[^{3}H]GDP by GDS. Rho·[^{3}H]GDP (5 μM) was equilibrated with GDS (0−15 μM) at 30 °C and filtered over a Centricon 10 membrane as described in the text. [^{3}H]GDP concentrations in the filtrate were measured by liquid scintillation counting. The line is a smooth joining of the data points.

mantGDP was included in the analysis described subsequently. The observed mant fluorescence decreased, which is consistent with the formation of free mantGDP. The fluorescence intensity approached a minimum value at high GDS concentrations which was higher than expected if all the mantGDP had been displaced, indicating that some nucleotide remained bound. The addition of a large excess of GDP at the end of each titration caused a further decrease in intensity to a value expected for the complete displacement of bound mantGDP ($F_{Rho{\cdot}mantGDP} = 3.66F_{mantGDP}$ under these experimental conditions). These observations are consistent with the formation of a ternary complex between Rho·mantGDP and GDS from which mantGDP dissociates where $F_{Rho{\cdot}GDS{\cdot}mantGDP} > F_{mantGDP}$ (Scheme 1).

Scheme 1

$$Rho.mantGDP + GDS \rightleftharpoons Rho.GDS.mantGDP \rightleftharpoons Rho.GDS + mantGDP$$

Figure 1b shows data from a series of titrations where the Rho·GDS binary complex was added to mantGDP present at initial concentrations of 1, 5, and 10 μM. The emission intensity at 440 nm was recorded on excitation of the mant fluorophore at 366 nm. In this set of experiments, mantGDP was incorporated in the Rho·GDS stocks to prevent dilution of the nucleotide. The observed increase in mant fluorescence intensity is consistent with the formation of protein-bound mantGDP, either as a binary complex with Rho or in the ternary complex Rho·GDS·mantGDP (Scheme 1). A quantitative analysis of the data in Figure 1 is described subsequently in light of the kinetic results.

To confirm that the decrease in mant fluorescence when GDS interacts with Rho·mantGDP (Figure 1a) is associated with nucleotide dissociation, an ultrafiltration method was used to demonstrate that free nucleotide is formed when GDS interacts with Rho·[^{3}H]GDP (Figure 2). Mixtures of Rho·[^{3}H]GDP (5 μM) and GDS (0−15 μM) were allowed to reach equilibrium, and the free [^{3}H]GDP concentration present in each was determined by filtering a small proportion of the mixture over a Centricon 10 kDa concentration membrane. After correction for membrane depletion, the concentration of [^{3}H]GDP in the filtrate provides a measure of $[[^3H]\text{-}GDP]_{free}$ in the retentate. As shown in Figure 2, the interaction of GDS with Rho·[^{3}H]GDP results in the displacement of [^{3}H]GDP. Furthermore, a proportion of [^{3}H]GDP remains

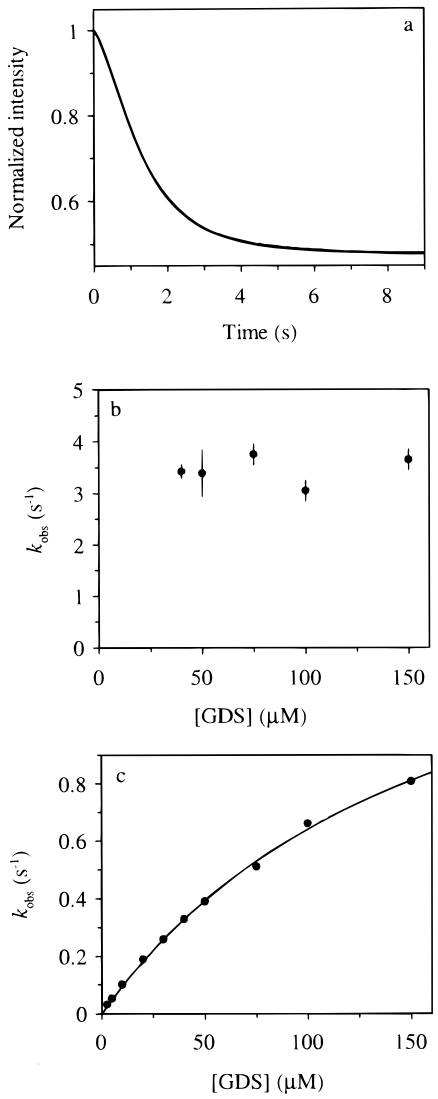

FIGURE 3: Kinetics of the interaction of excess GDS with Rho·mantGDP in the absence of exogenous GDP. (a) Rho·mantGDP (0.5 μM) was mixed with 150 μM GDS, and the mant fluorescence intensity was recorded (λ_{ex} = 366 nm). A fit of the time course to a double exponential ($k_{obs,1}$ = 3.56 s^{-1}, $k_{obs,2}$ = 0.81 s^{-1}) is superimposed. (b) Dependence of the observed rate constant describing the lag in the intensity decay illustrated above on GDS concentration. (c) Dependence of the observed rate constant of the intensity decrease illustrated above on GDS concentration.

bound at saturating GDS concentrations, indicating that under the conditions of this experiment the ternary complex is significantly populated.

Kinetics of the Interaction of Excess GDS with Rho·MantGDP. Stopped-flow experiments were performed to investigate the kinetics of the decrease in mant fluorescence observed when GDS interacts with Rho·mantGDP. An excess of GDS (2.5−150 μM) was mixed with Rho·mantGDP (0.5 μM), and the mant emission intensity was monitored on excitation of the mant fluorophore at 366 nm. The time course obtained at 150 μM GDS is shown in Figure 3a. The interaction of GDS with Rho·mantGDP was characterized by a decrease in intensity which is correlated to the release of bound mantGDP as discussed above. Time courses obtained at GDS concentrations between 2.5 and 30 μM were adequately fitted by a single exponential, although a small systematic deviation of the residuals could be seen. However, a lag phase in the intensity decay became more pronounced

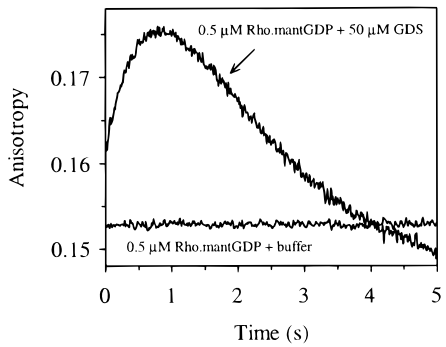

FIGURE 4: Anisotropy of mant fluorescence on mixing Rho·mantGDP with an excess of GDS. Rho·mantGDP (0.5 μM) was mixed with GDS (50 μM), and the anisotropy of mant fluorescence was followed on excitation at 366 nm. Data from a control experiment where Rho·mantGDP (0.5 μM) was mixed with buffer are shown.

at high GDS concentrations, and time courses obtained at ≥40 μM GDS were fitted to a double-exponential function with amplitude terms with opposite signs. The observed rate constants describing the lag phase were independent of GDS concentration at a value of ∼3.5 s^{-1} (Figure 3b). The observed rate constants of the decay phase exhibited a nonlinear dependence on GDS concentration (Figure 3c). The apparent second-order rate constant at low GDS concentrations calculated from the slope of the linear region of Figure 3c is 1 × 10^4 M^{-1} s^{-1}. As discussed above, the fluorescence decay phase is related to mantGDP dissociation from the ternary complex. The presence of a lag in the decay is consistent with this interpretation if the relative fluorescence of Rho·mantGDP is the same as that of the ternary complex Rho·GDS·mantGDP, i.e., if the binding of GDS to Rho·mantGDP (step 1 in Scheme 1) is spectroscopically silent. The experiment was repeated, but the fluorescence anisotropy was measured. Figure 4 shows the time dependence of the anisotropy of mant fluorescence when 0.5 μM Rho·mantGDP was mixed with 50 μM GDS. A transient increase in anisotropy was seen, followed by a slower decay. The observed rate constant of the transient increase in anisotropy (k_{obs} = 2.5 s^{-1}) is similar to the observed rate constant describing the lag phase seen in the intensity data. If there are no significant changes in the local motion of the mant fluorophore on binding of GDS to Rho·mantGDP, the transient increase in fluorescence anisotropy is consistent with ternary complex formation. The subsequent decay in anisotropy is in accord with the formation of free mantGDP, which has a fluorescence anisotropy of ∼0.025.

Kinetics of the Interaction of GDS with Rho·MantGDP in the Presence of Exogenous GDP. The interaction of GDS with Rho·mantGDP in the presence of exogenous GDP was also investigated. Rho·mantGDP (0.5 μM) was mixed with GDS (2.5−150 μM) which contained a large excess of GDP (100 μM) over Rho·mantGDP. The intensity of mant fluorescence was observed to decay (Figure 5a) in a manner similar to that found in the experiments performed in the absence of exogenous GDP. Time courses obtained between 2.5 and 10 μM GDS were adequately fitted by a single exponential, whereas data obtained at ≥20 μM GDS required a double exponential to accommodate a lag in the intensity decay which became more pronounced at higher GDS concentrations. The observed rate constant describing the lag phase increased from 1.5 s^{-1} at 20 μM GDS to 3 s^{-1} at 150 μM

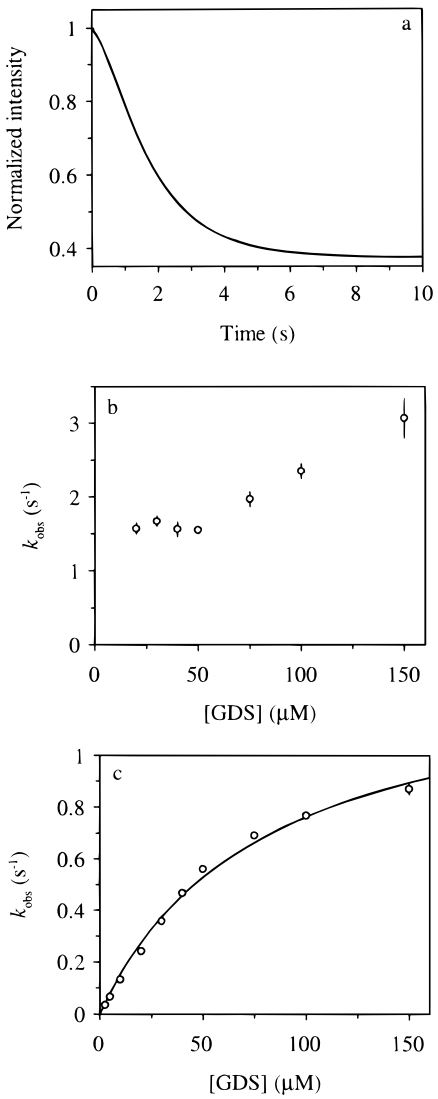

FIGURE 5: Kinetics of the interaction of GDS with Rho·mantGDP in the presence of exogenous GDP. (a) Rho·mantGDP (0.5 μM) was mixed with GDS (75 μM) containing a large excess of GDP (100 μM), and mant fluorescence was recorded on excitation at 366 nm. A fit of the time course to a double exponential ($k_{obs,1}$ = 1.91 s^{-1}, $k_{obs,2}$ = 0.69 s^{-1}) is superimposed. (b) Dependence of the observed rate constant describing the lag in the intensity decay illustrated above on GDS concentration. (c) Dependence of the observed rate constant of the intensity decay on GDS concentration. The line through the points is the best fit to eq 3, as described in the text.

GDS (Figure 5b). The observed rate constant of the decay phase exhibited a nonlinear dependency on GDS concentration (Figure 5c). An apparent second-order rate constant of 1.2×10^4 M^{-1} s^{-1} is given by the slope at low GDS concentrations. A maximum value for the observed rate constant of the decay phase at saturating GDS concentrations of ~1.4 s^{-1} was estimated from a fit of the data in Figure 5c to a simple hyperbola with an ordinate intercept of zero (eq 3). The amplitude of the decay phase was independent of GDS concentration which is consistent with Scheme 1 since in the presence of a large excess of unlabeled GDP complete displacement of mantGDP is expected at equilibrium.

Displacement of MantGDP from Rho·MantGDP/GDS at Equilibrium. To gain further information about the kinetics of mantGDP dissociation, an equilibrium mixture of Rho·mantGDP and GDS was rapidly mixed with an excess of

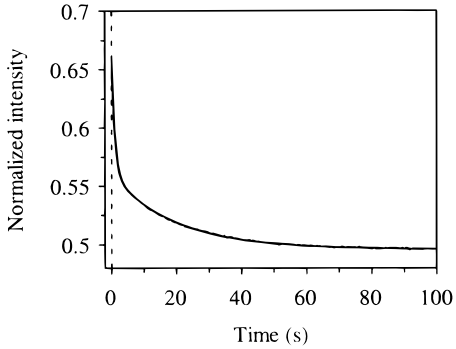

FIGURE 6: Kinetics of mantGDP displacement from a pre-equilibrated mixture of Rho·mantGDP and GDS. A mixture of Rho·mantGDP (0.5 μM) and GDS (5 μM) which had been incubated at 30 °C for 20 min was mixed with a large excess of GDP (100 μM). Mant fluorescence was recorded on excitation at 366 nm. The time course has been normalized relative to an intensity of one for the same experiment performed in the absence of GDS. A fit of the data to a double exponential ($k_{obs,1}$ = 0.96 s^{-1} and $k_{obs,2}$ = 0.051 s^{-1}) is shown.

GDP. Figure 6 shows data from an experiment where Rho·mantGDP (0.5 μM) was pre-equilibrated with GDS (5 μM) for 20 min before mixing with an excess of GDP (100 μM) in the stopped-flow apparatus. Mant fluorescence decayed biexponentially with the following observed rate constants: $k_{obs,1}$ = 0.96 s^{-1} and $k_{obs,2}$ = 0.051 s^{-1}. This observation is consistent with Scheme 1 if $F_{Rho\cdot mantGDP} = F_{Rho\cdot GDS\cdot mantGDP} > F_{mantGDP}$, where the fast phase represents dissociation of mantGDP from the ternary complex. The slow phase of the mant intensity decrease is a consequence of the slow binding of GDS to Rho·mantGDP.

Kinetics of the Interaction of MantGDP with Rho·GDS. The availability of the Rho·GDS binary complex allowed the kinetics of the reverse reaction shown in Scheme 1 to be investigated. Sedimentation velocity and equilibrium experiments had previously confirmed the 1:1 stoichiometry of this complex (*26*). Rho·GDS (0.5 μM) was mixed with increasing concentrations of mantGDP, and mant fluorescence was recorded following excitation by energy transfer from tryptophan. There was a biphasic increase in fluorescence intensity comprising a fast phase which was complete within 200 ms and a slow phase which was complete within 100 s (Figure 7a). Both phases could be well fitted to a single exponential. The observed rate constant of the fast phase increased linearly with mantGDP concentration up to 50 μM (Figure 7b) with an ordinate intercept of ~3 s^{-1} and an apparent second-order rate constant at low mantGDP concentrations of 5×10^5 M^{-1} s^{-1}. However, at higher mantGDP concentrations, the observed rate constant of the fast phase reached a saturating value of 30 s^{-1}. The observed rate constant of the slow phase of the intensity increase exhibited a hyperbolic dependency on mantGDP concentration (Figure 7c). This plot was fitted to eq 3 with a non-zero intercept to give the observed rate constant at saturation of 0.078 s^{-1}, with an ordinate intercept of 0.034 s^{-1} and a $K_{d,app}$ of 26 ± 3 μM. Consideration of the amplitude terms of the observed processes is complicated by the large background signal and attenuation of the excitation light by mantGDP absorption. However, at each mantGDP concentration, the amplitudes of the two phases were approximately the same as each other. The possibility that the use of excitation by energy transfer was contributing an extra signal was investigated in a control

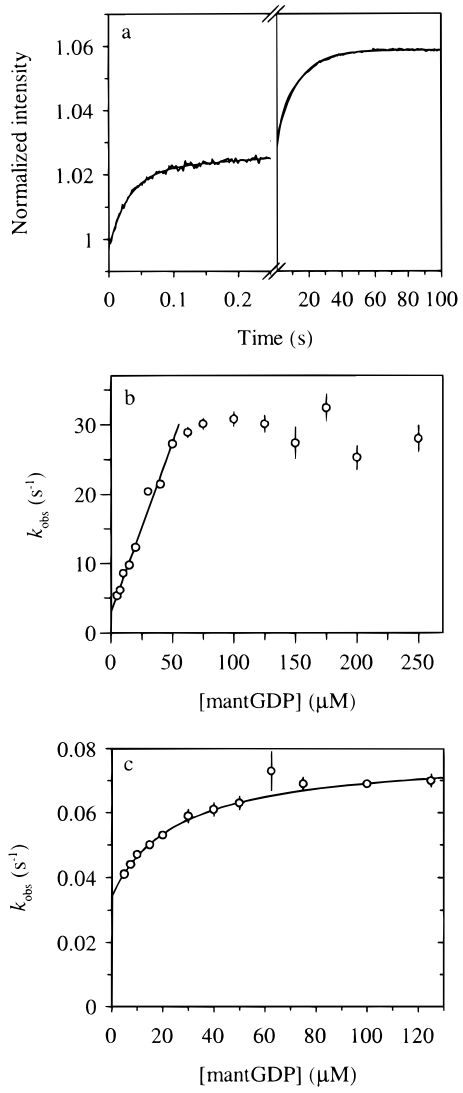

FIGURE 7: Kinetics of the interaction of mantGDP with Rho·GDS. (a) Rho·GDS (0.5 μM) was mixed with mantGDP (100 μM), and mant fluorescence was recorded on excitation at 280 nm. Data for the first 250 ms of the reaction were fitted to a single exponential (k_{obs} = 31 s^{-1}) with a slope to accommodate the early part of the slower phase. Data between 0.5 and 100 s were fitted to a single exponential (k_{obs} = 0.069 s^{-1}). (b) Dependence of the observed rate constant of the fast phase of mant intensity increase on mantGDP concentration. Data between 5 and 50 μM mantGDP have been fitted to a straight line, with an intercept of 3 s^{-1} and a slope of 5 × 10^5 M^{-1} s^{-1}. (c) Dependence of the observed rate constant of the slow phase of mant intensity increase on mantGDP concentration. The solid line is the best fit to eq 3 as described in the text.

experiment where mantGDP (0.5 μM) was mixed with excess Rho·GDS complex (5 μM) with excitation at 366 nm. Again, two phases of the intensity increase were seen (data not shown), of observed rate constants 3.0 and 0.033 s^{-1}, irrespective of whether the sample was excited at 366 or 280 nm. These values compare well with those measured under conditions of excess mantGDP shown in Figure 7 (5.3 and 0.041 s^{-1} at 5 μM mantGDP).

Isomerization of MantGDP. Nucleotides modified at the ribose ring with the mant fluorophore exist as a mixture of 2′-*O* and 3′-*O* isomers which interconvert within minutes at physiological pH (*24*, *34*, *35*). The equilibrium ratio of 2′-*O* isomer to 3′-*O* isomer for mantADP has been determined to be 35:65 (*36*). The interconversion of the 2′ and 3′ isomers

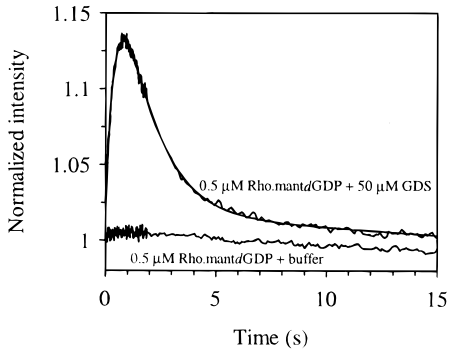

FIGURE 8: Kinetics of the interaction of Rho·mant*d*GDP with excess GDS. Rho·mant*d*GDP (0.5 μM) was mixed with GDS (50 μM), and the fluorescence intensity was recorded (λ_{ex} = 366 nm). The time course was fitted to a double exponential ($k_{obs,1}$ = 2.0 s^{-1}, $k_{obs,2}$ = 0.68 s^{-1}) incorporating a slope to account for photobleaching. Data from a control experiment where Rho·mant*d*GDP (0.5 μM) was mixed with buffer are shown.

of mantADP at pH 7.5, extrapolated to the temperature of the experiments reported here, occurs at a rate of ~0.016 s^{-1} (*35*). To test whether the biphasic kinetics observed when mantGDP was mixed with Rho·GDS (Figure 7) were a consequence of the two isomers, the mant derivative of 2′-deoxyGDP was synthesized in which isomerization cannot occur. Energy transfer between tryptophan in Rho and the mant fluorophore in the Rho·mant*d*GDP complex was observed (data not shown). However, in contrast to the situation with mantGDP, the emission spectra of Rho-bound and free mant*d*GDP on excitation at 366 nm were very similar, suggesting that the large intensity enhancement seen on binding of mantGDP to Rho originated from the bound isomer with the mant group attached at the 2′-position. The rate constant for dissociation of mant*d*GDP from Rho was measured by displacement with a large excess of GDP. In the absence of a significant intensity difference between the bound and free forms of the nucleotide, the anisotropy of mant fluorescence was used to monitor dissociation. The decrease in anisotropy from ~0.170 to ~0.020 observed after mixing 1 μM Rho·mant*d*GDP with 100 μM GDP at 30 °C was well described by a single exponential, giving a dissociation rate constant of (3.2 ± 0.03) × 10^{-4} s^{-1}. This rate constant is similar to those measured for Rho·mantGDP (k_{diss} = 2.0 × 10^{-4} s^{-1}) and Rho·GDP (k_{diss} = 1.2 × 10^{-4} s^{-1}). The two phases of the intensity increase on mixing mantGDP with Rho·GDS (Figure 7) were not a consequence of using mixed isomer mantGDP since two phases of the intensity increase of similar observed rates were also seen in corresponding experiments with mant*d*GDP (data not shown). However, the accessible concentration range with this nucleotide was more restricted due to the weaker signals.

In an experiment analogous to that illustrated for Rho·mantGDP in Figure 3, Rho·mant*d*GDP was mixed with a large excess of GDS (50 μM). The observed time course comprised a transient increase in intensity followed by a slower decay in the fluorescence to approximately the value at the start of the reaction (Figure 8). This is consistent with Scheme 1 if $F_{Rho\cdot GDS\cdot mantdGDP} > (F_{Rho\cdot mantdGDP} \approx F_{mantdGDP})$. The time course was described well by a double-exponential function, incorporating a slope to account for photobleaching, with a k_{obs} of 2.0 s^{-1} for the transient increase and a k_{obs} of 0.68 s^{-1} for the decay. These observed rate constants are

comparable to those describing the lag phase and intensity decay, respectively, seen when Rho·mantGDP was mixed with 50 μM GDS ($k_{obs,lag} = 3.4$ s^{-1} and $k_{obs,decay} = 0.39$ s^{-1}, Figure 3). The results obtained with Rho·mant*d*GDP therefore reinforce the interpretation of the lag phase observed when Rho·mantGDP interacts with GDS.

Kinetics of the Interaction of GDP with Rho·GDS. To provide further support for the use of mantGDP as an analogue of the native ligand, the interaction of GDP with Rho·GDS was also investigated. This could be followed using the fluorescence of the extrinsic dye ANS, which acts as a probe for the extent of exposure of hydrophobic regions in proteins (*37*). When Rho·GDS (0.5 μM) containing ANS (10 μM) was mixed with excess GDP, a biphasic decrease in the intensity of ANS fluorescence was observed (data not shown). The observed rate constants of the slow phase exhibited a hyperbolic dependency on GDP concentration in the range of 2.5−375 μM. These data were fitted to eq 3 with a non-zero intercept to give a $K_{d,app}$ of 22.5 μM, an intercept of 0.005 s^{-1}, and an observed rate constant at saturation of 0.042 s^{-1}. A full concentration dependency of the fast phase of the ANS fluorescence decrease was not obtained. At 50 μM GDP, the observed rate constant of this phase was 18 s^{-1}, which compares to an observed rate constant of 27 s^{-1} for the fast phase of the mant intensity increase seen when Rho·GDS was mixed with 50 μM mantGDP.

The interaction of GDP with Rho·GDS could also be followed using tryptophan fluorescence. An increase in intensity was observed which was described well by a single exponential. The observed rate constants also exhibited a hyperbolic dependency on GDP concentration (data not shown). These data were fitted to eq 3 with a non-zero intercept to give a $K_{d,app}$ of 11 μM, an intercept of 0.005 s^{-1}, and an observed rate constant at saturation of 0.040 s^{-1}. A rapid phase of the tryptophan intensity decrease of very small amplitude was detected at high GDP concentrations but could not be characterized further. The processes reported by ANS and tryptophan fluorescence are very similar to each other and bear a quantitative similarity to both phases of mant fluorescence increase seen when Rho·GDS was mixed with mantGDP (Figure 7).

ANALYSIS AND SIMULATIONS

A full understanding of the mechanism by which GDS accelerates nucleotide release from Rho requires the characterization of intermediates in the mechanism and an assignment of individual rate constants to the proposed steps. All steps must be treated as reversible since nucleotide exchange requires the reaction to proceed readily in both directions.

Binding of GDS to Rho·MantGDP. The observed rate constant of the lag in the mant intensity decay when excess GDS was mixed with Rho·mantGDP (~3.5 s^{-1}, Figure 3b) was independent of GDS concentration in the range studied and is proposed to characterize the dissociation of mantGDP from Rho·GDS·mantGDP (step 2 in Scheme 1, where $F_{Rho·mantGDP} = F_{Rho·GDS·mantGDP} > F_{mantGDP}$). The observed rate constants of the decay phase exhibited a strong dependency on GDS concentration (Figure 3c) and are therefore proposed to characterize the association of GDS with Rho·mantGDP (step 1 in Scheme 1). A similar situation has been described for the calcium-dependent bioluminescence of aequorin (*38*), where a transient increase in concentration of an intermediate formed after calcium binding to the protein, followed by a slow decay of this intermediate, is characterized by a slower rate constant for formation of the intermediate than for its decay. At low GDS concentrations, the observed rate constant of the decay phase is limited by slow association of GDS with Rho·mantGDP occurring with a second-order rate constant of 1×10^4 M^{-1} s^{-1}. As the GDS concentration is increased, the kinetics of the decay in mant fluorescence become increasingly limited by mantGDP dissociation (step 2). For the experiments performed in the presence of excess GDP (Figure 5), where mantGDP rebinding after dissociation is negligible, the decay phase at saturating GDS concentrations is expected to occur at an observed rate constant of 1 s^{-1}, in accord with the fast phase of the mant intensity decrease seen when a pre-equilibrated mixture of Rho·mantGDP and GDS was mixed with excess GDP (Figure 6). These saturating concentrations of GDS were not achieved in practice. Since the observed rate constants of the two processes (lag and decay) illustrated in Figures 3 and 5 are of similar magnitude, the two steps reported will be coupled to some extent at intermediate GDS concentrations and the rate constants of the observed processes will be a complex function of individual rate constants.

Binding of MantGDP to Rho·GDS. In the analysis described above, a change in mant fluorescence is assumed to occur at step 2 in Scheme 1. This predicts that on mixing Rho·GDS with excess mantGDP there would be an exponential increase in fluorescence, the observed rate constant of which would be linearly dependent on mantGDP concentration. However, as shown in Figure 7, two phases of intensity increase were seen and the observed rate constants of both reached saturating values. The simplest interpretation of this behavior is that the association of mantGDP with Rho·GDS occurs in a two-step process where initial complex formation, which is spectroscopically silent, is followed by a conformational change within the ternary complex. Thus, the reaction sequence was extended as shown in Scheme 2,

Scheme 2

$$\text{Rho.mantGDP} + \text{GDS} \underset{k_{-1}}{\overset{k_1}{\rightleftharpoons}} \text{Rho.GDS.mantGDP} \underset{k_{-2}}{\overset{k_2}{\rightleftharpoons}} \text{Rho*.GDS.mantGDP} \underset{k_{-3}}{\overset{k_3}{\rightleftharpoons}} \text{Rho*.GDS} + \text{mantGDP}$$

where the fluorescence change occurs at step 2, i.e., ($F_{Rho·mantGDP} = F_{Rho·GDS·mantGDP}$) > ($F_{Rho*·GDS·mantGDP} = F_{mantGDP}$).

At low mantGDP concentrations, the observed rate constant of the fast fluorescence change when excess mantGDP was mixed with Rho·GDS (Figure 7) is limited by slow binding of mantGDP to Rho·GDS with a second-order rate constant of 5×10^5 M^{-1} s^{-1} (k_{-3}) given by the slope of the line shown in Figure 7b. The *y*-axis intercept of ~3 s^{-1} provides an estimate of k_3 in Scheme 2. This value is consistent with the observed rate constant describing the lag phase seen on interaction of GDS with Rho·mantGDP (~3.5 s^{-1}) which was proposed to characterize mantGDP dissociation from the ternary complex. The observed rate constant of the fast phase of the intensity increase at high mantGDP concentrations (30 s^{-1}, Figure 7b) thus represents the sum of the forward and reverse rate constants for ternary complex

isomerization ($k_2 + k_{-2}$). The observed rate constants of the two phases shown in Figure 7 are sufficiently different to assume that the two steps are not highly coupled; i.e., the initial equilibration of step 2 is essentially independent of the subsequent equilibration of step 1. The slow phase of intensity increase (Figure 7c) is a consequence of the dissociation of GDS from the ternary complex. This interpretation was confirmed in a control experiment where mantGDP (0.5 μM) was mixed with a solution of Rho·GDS (5 μM) which contained a large excess of GDS (50 μM). Only a single phase of the mant intensity increase was observed ($k_{obs} = 3.0\ s^{-1}$), which originates from the equilibration of step 2 (data not shown). The absence of a slower phase of increase is a result of the large excess of GDS preventing GDS dissociation at step 1. In Figure 7c, the net dissociation rate of GDS at saturating mantGDP concentrations ($k_{off} = 0.078\ s^{-1}$), neglecting the small contribution from association at step 1, is approximated by the relation $k_{off} = k_{-1}k_{-2}/(k_2 + k_{-2})$, provided $(k_2 + k_{-2}) \gg k_{-1}$.

Data from the displacement experiment where a preequilibrated mixture of Rho·mantGDP (0.5 μM) and GDS (5 μM) was mixed with excess GDP (Figure 6) can be used to achieve an approximate resolution of $k_2 + k_{-2}$. The fast phase of mant intensity decrease ($k_{off} = 0.96\ s^{-1}$, Figure 6) is related to the individual rate constants in Scheme 2 by the relation $k_{off} = k_2k_3/(k_2 + k_{-2})$, provided $(k_2 + k_{-2}) \gg k_3$. From $k_2 + k_{-2} = 30\ s^{-1}$ and $k_3 \sim 3.5\ s^{-1}$, we estimate $k_2 \sim 9\ s^{-1}$ and thus $k_{-2} \sim 21\ s^{-1}$. The slow phase of the intensity decrease shown in Figure 6 ($k_{obs} = 0.051\ s^{-1}$) is a consequence of the slow binding of GDS to Rho·mantGDP and occurs at an observed rate at 5 μM GDS which is consistent with an apparent second-order rate constant (k_1) of $1 \times 10^4\ M^{-1}\ s^{-1}$.

Analysis of GDS Binding to Rho·MantGDP by Numerical Methods. Refined estimates of k_1, k_2, and k_3 were obtained by a global numerical analysis of the kinetic data obtained for the interaction of GDS with Rho·mantGDP in the presence of excess exogenous GDP shown in Figure 5. In this approach, sets of kinetic data obtained under different concentration conditions are simultaneously fitted using differential equations describing the proposed mechanism, in this case Scheme 2. The use of global methods has been discussed elsewhere (*39*, *40*), and when applied to kinetic data, they have the advantage that the amplitude information is explicitly included in the analysis. However, slight variations in the amplitudes of processes measured in the stopped-flow apparatus, due to either instrumental drift or experimental artifacts, can be a limitation. This problem could be addressed in the experiments where GDS was mixed with Rho·mantGDP in the presence of excess GDP (Figure 5), since the dissociation of mantGDP proceeds to completion at all GDS concentrations. Thus, the time courses at each GDS concentration were individually normalized to give an intensity change of 1 by dividing by the total amplitude of the change obtained from the exponential analysis. Time courses were then scaled to a starting intensity of 1. This treatment preserves the relative amplitude of the two phases of the mant fluorescence change seen at each GDS concentration.

Normalized time courses obtained for the reaction of 0.5 μM Rho·mantGDP with GDS (10−150 μM) in the presence of 100 μM GDP were fitted to Scheme 2, where the spectroscopic change is assumed to occur at step 2. In this analysis, the values of k_{-2} and k_{-1} were constrained by the relationships $k_2 + k_{-2} = 30$ and $k_{-1}k_{-2}/(k_2 + k_{-2}) = 0.078$. Since rebinding of mantGDP is in effect abolished by the large excess of GDP, k_{-3} was assigned a value of zero. The best-fit values for the three variable parameters in this analysis were as follows: $k_1 = 1.6 \times 10^4\ M^{-1}\ s^{-1}$, $k_2 = 6.1 \pm 0.1\ s^{-1}$, and $k_3 = 5.2 \pm 0.1\ s^{-1}$. As shown in Figure 9, the simulated time courses faithfully reproduce the lag and decay observed in the experimental data. Although slight systematic deviations were observed in the fit, particularly at low GDS concentrations, the overall quality of the fit was good considering that kinetic data obtained over a 15-fold range of GDS concentrations were simultaneously analyzed. The rate constants obtained from the combined analysis of the data by Scheme 2 are summarized in Table 1. These rate constants were used to simulate time courses of mant fluorescence for the interaction of mantGDP with Rho·GDS, according to Scheme 2 where the spectroscopic change occurs at step 2. The simulated data showed a biphasic increase in signal, in accord with the experimental data (Figure 7a). The simulated time courses were fitted to two exponentials to give "observed" rate constants which showed a dependency on mantGDP concentration similar to that of the experimental observed rate constants (Figure 7b,c) and were within 30% of the respective experimental values.

Quantitative Analysis of Equilibrium Titration Data. The minimal mechanism developed above (Scheme 2) was used to make a quantitative analysis of the titration data in Figure 1 by global numerical methods. A similar approach has been used for analyzing the binding of the exchange factor GrpE

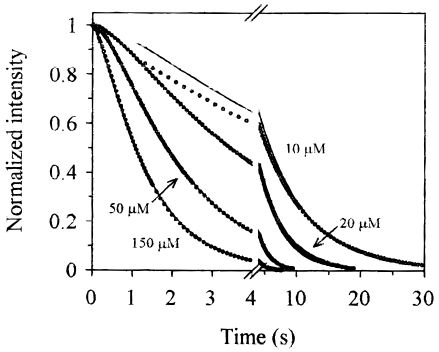

FIGURE 9: Numerical analysis of the kinetic data for the interaction of GDS with Rho·mantGDP in the presence of exogenous GDP. Time courses of mant fluorescence obtained on mixing Rho·mantGDP (0.5 μM) with GDS (10−150 μM) containing exogenous GDP (100 μM) were normalized and scaled as described in the text. Data were globally analyzed according to Scheme 2 using the rate constants given in the text. Data (circles) and fitted curves are shown for four representative GDS concentrations.

Table 1: Rate Constants for the Proposed Minimal Mechanism of GDS-Stimulated MantGDP Dissociation from Rho (Scheme 2)[a]

k_1	$1.6 \times 10^4\ M^{-1}\ s^{-1}$ [b]	k_{-2}	$23.9\ s^{-1}$ [c]
k_{-1}	$0.098\ s^{-1}$ [c]	k_3	$5.2\ s^{-1}$ [b]
k_2	$6.1\ s^{-1}$ [b]	k_{-3}	$5 \times 10^5\ M^{-1}\ s^{-1}$ [d]

[a] Rate constants were obtained by a combination of traditional and global kinetic analysis of stopped-flow data for the interaction of GDS with Rho·mantGDP and mantGDP with Rho·GDS as described in the text. [b] From a global fit. [c] Constrained in a global fit as described. [d] From Figure 7b.

Scheme 3

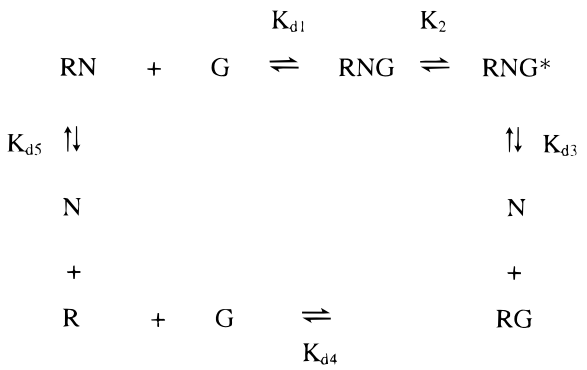

to the DnaK·ADP complex (*41*) and the exchange factor Cdc25^{Mm} to H-Ras·GDP (*22*). For this treatment, Scheme 2 was extended into the thermodynamic cycle of coupled equilibria shown in Scheme 3, where R is Rho, N is mantGDP, and G is GDS.

The equilibrium constants are defined as follows: K_{d1} = [RN][G]/[RNG], K_2 = [RNG*]/[RNG], K_{d3} = [RG][N]/[RNG*], K_{d4} = [R][G]/[RG], and K_{d5} = [R][N]/[RN]. Since the equilibria are coupled, any one equilibrium constant can be expressed in terms of the other four. The analysis model was constructed from the above definitions of K_{d1}, K_2, K_{d3}, and K_{d5} where $K_{d4} = (K_{d1}K_{d5})/(K_2K_{d3})$. Conservation of mass equations related the known total concentrations to those of the individual species. The observed fluorescence was expressed as the sum of the concentration of each species multiplied by a parameter defining its relative fluorescence. For the titrations of GDS into Rho·mantGDP, where the emission intensity was monitored at 430 nm, $F_{RN} = F_{RNG} = 3.66F_{RNG*} = 3.66F_N$. For the titrations of Rho·GDS into mantGDP, where emission intensity was monitored at 440 nm, $F_{RN} = F_{RNG} = 3.22F_{RNG*} = 3.22F_N$. Due to the very high affinity of Rho for mantGDP, the free Rho concentration is negligible under the conditions of the titrations reported here and thus K_{d5} is not constrained. An experimental value for K_{d5} is not available due to the instability of the nucleotide-free protein. However, a second-order association rate constant of 2.5×10^7 M^{-1} s^{-1} at 30 °C for the binding of GDP to N-Ras can be estimated by extrapolation from low-temperature measurements (*42*). If a similar value is assumed for the binding of mantGDP to Rho, a dissociation constant of ~10 pM for Rho·mantGDP can be estimated on the basis of the measured dissociation rate constant of 2.0×10^{-4} s^{-1}. K_{d5} was thus held constant during the analysis at 10 pM. However, fixing K_{d5} at values up to 1 nM had a negligible effect on the fitted values of K_{d1}, K_2, and K_{d3}.

The best-fit values of the three variable parameters in this analysis, as defined above, were as follows: K_{d1} = 5.8 ± 1.2 μM, K_2 = 0.50 ± 0.06, and K_{d3} = 6.7 ± 1.9 μM. As shown in Figure 1, the overall quality of the fit was good considering that data from seven different titrations performed on the exchange reaction in both directions were simultaneously analyzed. Furthermore, these values correspond well with those calculated from the kinetic data in Table 1 (K_{d1} = 6.1 μM, K_2 = 0.26, K_{d3} = 10.4 μM). The analysis of the titration data was based on Scheme 2, the minimal mechanism needed to explain the kinetic data, where the fluorescence change occurs at step 2. However, the analysis is independent of the rate constants (and hence equilibrium constants) obtained from the kinetic data. The relative fluorescence of RNG and RNG* could not be treated as variable parameters in the equilibrium analysis since their values are too highly correlated to those of the equilibrium constants.

DISCUSSION

The availability of high concentrations of soluble GDS and a well-characterized Rho·GDS complex has allowed the interaction of GDS with Rho·mantGDP to be studied under a wide range of conditions. Both equilibrium and kinetic measurements could be made on the reaction in either direction. Most studies were performed with the fluorescent GDP analogue, mantGDP, either by direct excitation of its fluorescence at 366 nm or by energy transfer from tryptophan excited at 280 nm. MantGDP exists as an equilibrium mixture of the 2′-O- and 3′-O-substituted nucleotides which may complicate the analysis, whereas mant*d*GDP exists as a single species. MantGDP was chosen for most experiments because it gave much larger fluorescence changes in the mechanism. However, some experiments were performed with mant*d*GDP which showed that the biphasic fluorescence processes seen with mantGDP were not due to the presence of two isomers. Furthermore, experiments in which GDP itself was used and either intrinsic tryptophan fluorescence or extrinsic ANS fluorescence was monitored, where appropriate, showed that mantGDP behaved very much like GDP in this system.

The main conclusion of this study is that the mechanism of release of mantGDP from Rho catalyzed by GDS is a substituted enzyme mechanism which involves a conformational change within the Rho·GDS·mantGDP ternary complex (Scheme 2). Strong support for the proposed mechanism is given by the fact that using the rate constants determined for Scheme 2 (Table 1) and the step assigned as giving a change in fluorescence, simulations of the experiments in which the reaction is initiated in both directions show a close correlation to the concentration dependency of the experimentally observed rate constants. Furthermore, values of K_{d1}, K_2, and K_{d3} determined by equilibrium titration were in close agreement with the kinetic data. The equilibrium constant (K_0) for the overall reaction

$$\text{Rho·mantGDP} + \text{GDS} \rightleftharpoons \text{Rho·GDS} + \text{mantGDP}$$

where K_0 = ([Rho·GDS][mantGDP])/([Rho·mantGDP][GDS]) obtained from the equilibrium titration data has a value of 0.58. The overall equilibrium constant derived from the elementary rate constants shown in Table 1, where $K_0 = k_1k_2k_3/k_{-1}k_{-2}k_{-3}$, is 0.43.

This value of K_0 can be compared to that for other guanine nucleotide exchange factors. Using rapid equilibrium isotope exchange measurements, Chau et al. (*13*) obtained a value of 2.8 for the EF-Tu/EF-Ts system. Eccleston (*14*), using a chromophoric analogue of GDP in the same system, calculated a value of 95, although since the analogue bound to EF-Tu approximately 80-fold weaker than GDP it was considered to be consistent with the results of Chau et al. (*13*). More recent work has concentrated on the Ras superfamily of proteins. Using techniques similar to those used in this study, Klebe et al. (*21*) determined the kinetic parameters for RCC1-stimulated mant*d*GDP dissociation

from Ran. A corresponding value for K_0 of 2.6 can be calculated from their data. In all of these systems, it therefore appears that the equilibrium between nucleotide-bound and exchange factor-bound complexes with the G-protein is close to unity so that the reaction can readily proceed in either direction, as determined by the local concentration of the individual components. However, the situation is different in the Ras/Cdc25 system (*22*), where a value for K_0 of 0.0015 can be calculated from the equilibrium constants determined from a combination of individual experiments and global fitting. This results from Cdc25 binding much more weakly to Ras·GDP than GDP binding to Ras·Cdc25, favoring the Ras·GDP complex. The data presented here and those published for the interaction of other exchange factors with the Ras superfamily of G-proteins are incompatible with the sequential mechanism proposed for eIF2-B (*23*) which would require the presence of exogenous nucleotide for dissociation of mantGDP to be observed.

The maximal rate of mantGDP dissociation from Rho in the presence of exogenous GDP and saturating concentrations of GDS is 1 s^{-1}. This represents a 5000-fold enhancement of the intrinsic rate of mantGDP dissociation from Rho. This can be compared to a maximum rate of 21 s^{-1} determined for the dissociation of mant*d*GDP from Ran in the presence of a large excess of GDP and high concentrations of the exchange factor RCC1 (*21*), which constitutes an enhancement of the intrinsic dissociation process by a factor of $\sim 10^6$. Lenzen et al. (*22*) determined a maximal rate constant of 3.9 s^{-1} for the release of Ras-bound mant*d*GDP catalyzed by $Cdc25^{Mm}$ under multiple-turnover conditions, which represents an enhancement of the intrinsic process by (2×10^5)-fold. However, under multiple-turnover conditions, the steady-state rate of GDS-stimulated nucleotide dissociation from Rho will be limited by the slow dissociation rate constant of GDS from the ternary complex ($k_{-1} = 0.098\ s^{-1}$) which only represents a 500-fold activation of the nucleotide release step. Clearly, in vivo, actual nucleotide dissociation rates depend critically on the local concentrations of the G-proteins, exchange factors, and free nucleotide.

Although the kinetic model involving an isomerization of the Rho·GDS·mantGDP ternary complex fits the data well, the apparent second-order rate constants for association of GDS with Rho·mantGDP and mantGDP with Rho·GDS are both much slower than rate constants for typical diffusion-controlled interactions (*43*). This could reflect particularly unfavorable steric or electrostatic components in the binding steps (*28*, *44*) or could be the result of both binding steps being more complex. All of the experimental data could be equally well, but not better, fitted to a model involving two conformational changes within the ternary complex and second-order rate constants of $> 10^6\ M^{-1}\ s^{-1}$. However, the minimal mechanism proposed in Scheme 2 is sufficient at present to account for the experimental results.

The formation of a ternary complex Rho·GDS·mantGDP indicates that the binding sites for the nucleotide and exchange factor on Rho are distinct. Thus, there is an implicit requirement for conformational change within the nucleotide binding site of Rho after the association of GDS for stimulated nucleotide dissociation to occur. For the Ran/RCC1 system, a simple mechanism analogous to Scheme 1 was sufficient to account for the data, although the authors raised the possibility of successive conformational changes occurring within the ternary complex from a state where RCC1 is weakly bound to a state where nucleotide is weakly bound (*21*). In the kinetic study of the Ras/$Cdc25^{Mm}$ system, Lenzen et al. (*22*) demonstrated two-step binding of mant*d*GDP to the Ras·$Cdc25^{Mm}$ complex and concluded that the second step constituted isomerization to a state with high nucleotide affinity. The forward and reverse rate constants determined for this conformational change were 21 and 3.9 s^{-1}, which bear a striking similarity to the corresponding rate constants determined in this study (k_{-2} and k_2, respectively, in Scheme 2). These authors also suggested that the association of $Cdc25^{Mm}$ with Ras·mant*d*GDP could be a multistep process but due to the insolubility of the exchange factor at high concentrations could not investigate this further. Ternary complex isomerization has been proposed for other exchange factors which operate by a substituted enzyme mechanism. Eccleston et al. (*17*), using pressure relaxation experiments on the EF-Tu/EF-Ts system, found evidence for an isomerization of the EF-Tu·EF-Ts·GDP ternary complex occurring before the release of GDP, and Packschies et al. (*41*) concluded that a conformational change follows the weak association of the exchange factor GrpE with DnaK·ADP.

This study does not address whether GDS selectively stimulates the dissociation of Rho-bound GDP in preference over GTP. Cdc25 has been shown to be more active against the GDP-bound state of Ras (*45*), whereas RCC1 causes a similar stimulation of nucleotide release from Ran·GDP and Ran·GTP (*21*). Work is underway to determine the corresponding kinetic parameters for the interaction of GDS with Rho·mantGTP and the interaction of mantGTP with Rho·GDS. The unusual substrate specificity of GDS is being addressed in kinetic and structural studies of its interaction with other Ras superfamily proteins.

ACKNOWLEDGMENT

We thank Y. Takai and A. Hall for kindly providing clones of bovine GDS and human RhoA, Jochen Reinstein and Howard White for helpful advice on the use of the program Scientist, Steve Howell for mass spectrometry, Phil Walker for performing the subcloning of GDS, and David Trentham, Robin Leatherbarrow, and Katrin Rittinger for helpful comments on the manuscript.

REFERENCES

1. Bourne, H. R., Sanders, D. A., and McCormick, F. (1991) *Nature 349*, 117−127.
2. Boguski, M. S., and McCormick, F. (1993) *Nature 366*, 643−654.
3. Quilliam, L. A., Khosravi-Far, R., Huff, S. Y., and Der, C. J. (1995) *BioEssays 17*, 395−404.
4. Yamamoto, T., Kaibuchi, K., Mizuno, T., Hiroyoshi, M., Shirataki, H., and Takai, Y. (1990) *J. Biol. Chem. 265*, 16626−16634.
5. Peifer, M., Berg, S., and Reynolds, A. B. (1994) *Cell 76*, 789−791.
6. Huber, A. H., Nelson, W. J., and Weis, W. I. (1997) *Cell 90*, 871−882.
7. Cherfils, J., Ménétrey, J., Mathieu, M., Le Bras, G., Robineau, S., Béraud-Dufour, S., Antonny, B., and Chardin, P. (1998) *Nature 392*, 101−105.
8. Mossessova, E., Gulbis, J. M., and Goldberg, J. (1998) *Cell 92*, 415−423.

9. Hiraoka, K., Kaibuchi, K., Ando, S., Musha, T., Takaishi, K., Mizuno, T., Asada, M., Ménard, L., Tomhave, E., Didsbury, J., Snyderman, R., and Takai, Y. (1992) *Biochem. Biophys. Res. Commun. 182*, 921−930.
10. Chuang, T.-H., Xu, X., Quilliam, L. A., and Bokock, G. M. (1994) *Biochem. J. 303*, 761−767.
11. Mizuno, T., Kaibuchi, K., Yamamoto, T., Kawamura, M., Sakoda, T., Fujioka, H., Matsuura, Y., and Takai, Y. (1991) *Proc. Natl. Acad. Sci. U.S.A. 88*, 6442−6446.
12. Kawamura, M., Kaibuchi, K., Kishi, K., and Takai, Y. (1993) *Biochem. Biophys. Res. Commun. 190*, 832−841.
13. Chau, V., Romero, G., and Biltonen, R. L. (1981) *J. Biol. Chem. 256*, 5591−5596.
14. Eccleston, J. F. (1984) *J. Biol. Chem. 259*, 12997−13003.
15. Hwang, Y. W., and Miller, D. L. (1985) *J. Biol. Chem. 260*, 11498−11502.
16. Romero, G., Chau, V., and Biltonen, R. L. (1985) *J. Biol. Chem. 260*, 6167−6174.
17. Eccleston, J. F., Kanagasabai, T. F., and Geeves, M. A. (1988)- *J. Biol. Chem. 263*, 4668−4672.
18. Pan, J. Y., and Wessling-Resnick, M. (1998) *BioEssays 20*, 516−521.
19. Boriack-Sjodin, P. A., Margarit, S. M., Bar-Sagi, D., and Kuriyan, J. (1998) *Nature 394*, 337−343.
20. Klebe, C., Bischoff, F. R., Ponstingl, H., and Wittinghofer, A. (1995) *Biochemistry 34*, 639−647.
21. Klebe, C., Prinz, H., Wittinghofer, A., and Goody, R S. (1995) *Biochemistry 34*, 12543−12552.
22. Lenzen, C., Cool, R. H., Prinz, H., Kuhlmann, J., and Wittinghofer, A. (1998) *Biochemistry 37*, 7420−7430.
23. Dholakia, J. N., and Wahba, A. J. (1989) *J. Biol. Chem. 264*, 546−550.
24. Jameson, D. M., and Eccleston, J. F. (1997) *Methods Enzymol. 278*, 363−390.
25. Self, A. J., and Hall, A. (1995) *Methods Enzymol. 256*, 3−10.
26. Hutchinson, J. P., Rittinger, K., and Eccleston, J. F. (2000) *Methods Enzymol. 325*, 71−82.
27. Hiratsuka, T. (1983) *Biochim. Biophys. Acta 742*, 496−508.
28. Fersht, A. (1998) *Structure and mechanism in protein science*, W. H. Freeman and Co., New York.
29. Sophianopoulos, A. J., and Sophianopoulos, J. A. (1985) *Methods Enzymol. 117*, 354−370.
30. Neal, S. E., Eccleston, J. F., and Webb, M. R. (1990) *Proc. Natl. Acad. Sci. U.S.A. 87*, 3562−3565.
31. Woodward, S. K. A., Eccleston, J. F., and Geeves, M. A. (1991) *Biochemistry 30*, 422−430.
32. Moore, K. J. M., and Lohman, T. M. (1994) *Biochemistry 33*, 14550−14564.
33. Hazlett, T. L., Moore, K. J. M., Lowe, P. N., Jameson, D. M., and Eccleston, J. F. (1993) *Biochemistry 32*, 13575−13583.
34. Rensland, H., John, J., Linke, R., Simon, I., Schlichting, I., Wittinghofer, A., and Goody, R. S. (1995) *Biochemistry 34*, 593−599.
35. Cheng, J.-Q., Jiang, W., and Hackney, D. D. (1998) *Biochemistry 37*, 5288−5295.
36. Cremo, C. R., Neuron, J. M., and Yount, R. G. (1990) *Biochemistry 29*, 3309−3319.
37. Brand, L., and Gohlke, J. R. (1972) *Annu. Rev. Biochem. 41*, 843−868.
38. Hastings, J. W., Mitchell, G., Mattingly, P. H., Blinks, J. R., and Van Leeuwen, M. (1969) *Nature 222*, 1047−1050.
39. Zimmerle, C. T., and Frieden, C. (1989) *Biochem. J. 258*, 381−387.
40. Beechem, J. M. (1992) *Methods Enzymol. 210*, 37−54.
41. Packschies, L., Theyssen, H., Buchberger, A., Bukau, B., Goody, R. S., and Reinstein, J. (1997) *Biochemistry 36*, 3417−3422.
42. Neal, S. E., Eccleston, J. F., Hall, A., and Webb, M. R. (1988) *J. Biol. Chem. 263*, 19718−19722.
43. Gutfreund, H. (1995) *Kinetics for the life sciences*, Cambridge University Press, Cambridge, U.K.
44. Koren, R., and Hammes, G. G. (1976) *Biochemistry 15*, 1165−1171.
45. Jacquet, E., Baouz, S., and Parmeggiani, A. (1995) *Biochemistry 34*, 12347−12354.

BI0007573